

Supporting Information

Nanostructured copper foam electrodes boost redox kinetics and suppress chemical side reactions of viologen anolytes in pH-neutral aqueous organic redox flow batteries

Yu Si ^{a,‡}, Haiguang Gao ^{a,‡}, Ruoqing Sun ^a, Juan Xu,^{a*}, Yong-Miao Shen ^b, Yucheng Huang ^c and Jianyu Cao ^{a*}

^a *Jiangsu Key Laboratory of Advanced Catalytic Materials and Technology, School of Petrochemical Engineering, Changzhou University, Changzhou, 213164, China.*

^b *Department of Chemistry, Zhejiang Sci-Tech University, Hangzhou 310018, China.*

^c *College of Chemistry and Material Science, Anhui Normal University, Wuhu 241000, China.*

*Corresponding author. E-mail: jycao@cczu.edu.cn (J. Cao); cjytion@cczu.edu.cn (J. Xu)

‡ These authors contributed equally to this work.

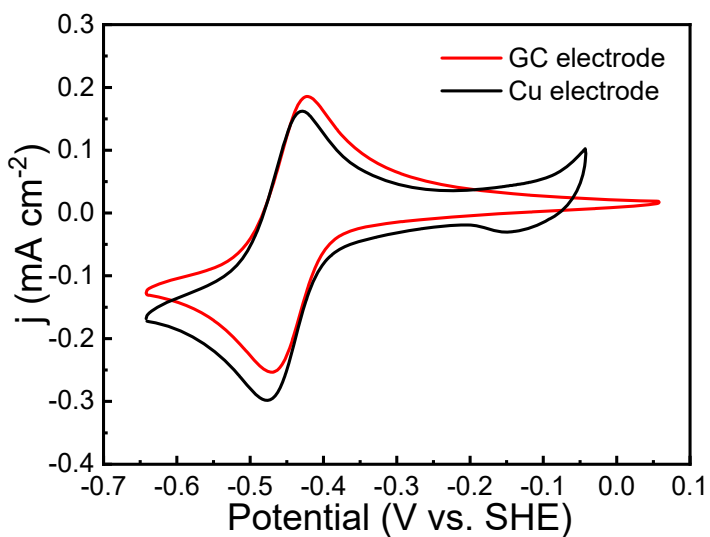


Fig. S1 CVs of MVCl_2 (2 mM) in 1 M NaCl solution at 50 mV s^{-1} on the GC and copper electrodes, respectively.

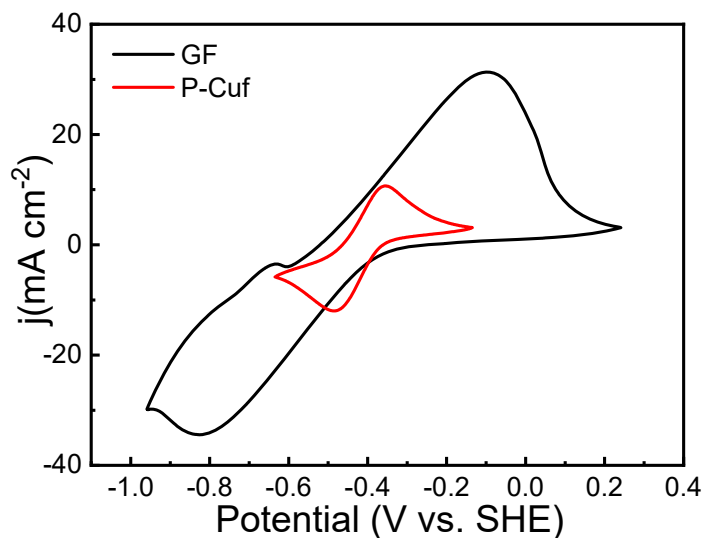


Fig. S2 CVs of MVCl_2 (10 mM) in 1 M NaCl solution at 50 mV s^{-1} on the GF and pristine copper foam (P-Cuf) electrodes, respectively.



Fig. S3 The photographic image of commercial P-Cuf.

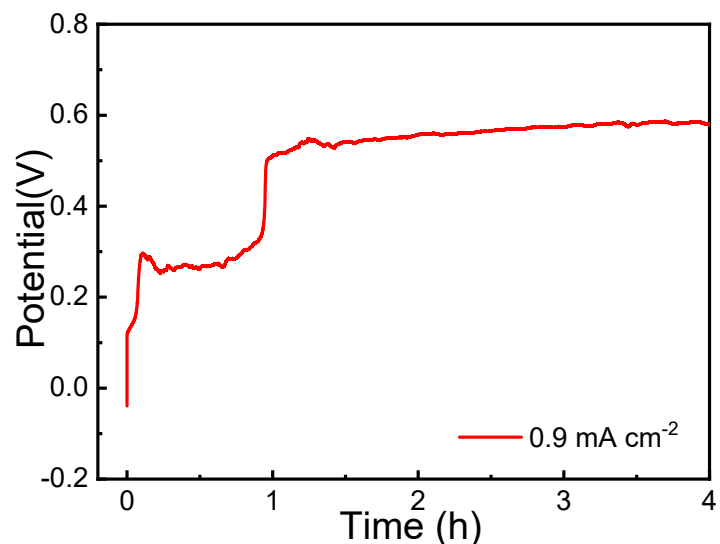


Fig. S4 The potential recorded in the electrochemical oxidation for a $1\text{ cm} \times 1\text{ cm}$ piece of the P-Cuf electrode at 0.9 mA cm^{-2} for 4 h in 1 M KOH solution.

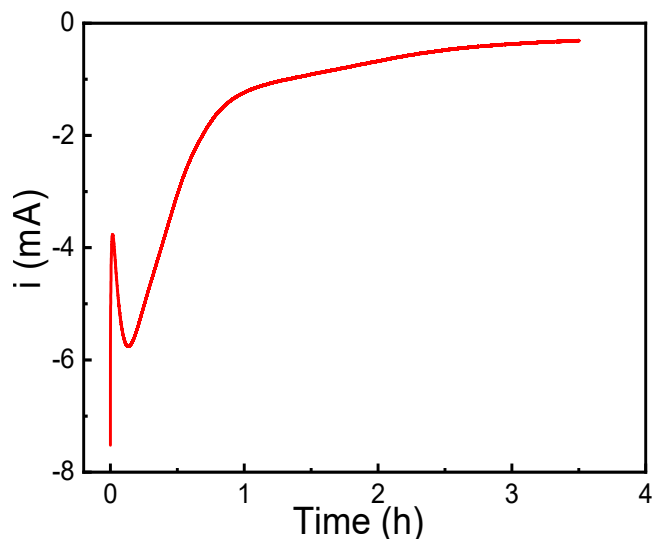


Fig. S5 The current recorded during the electrochemical reduction for a 1 cm × 1 cm piece of N-Cu₂O-j0.9 electrode at -0.4 V versus SHE in 1 M KHCO₃ solution.

Table S1 Surface roughness factors (SRFs) estimated from the non-Faradaic electrochemical capacitance measured by cyclic voltammetry. Cu-poly, polycrystalline Cu. NA, not applicable.

Sample	Oxidation current density (mA cm ⁻²)	C (mF cm ⁻²)	Surface Roughness Factor in reference to Cu-poly
Cu-poly disk	NA	0.12	1
P-Cuf	NA	1.17	9.80
N-Cuf-j0.52	0.52	9.32	77.7
N-Cuf-j0.78	0.78	12.72	106.0
N-Cuf-j0.9	0.9	20.41	170.1
N-Cuf-j1.3	1.3	19.13	159.5

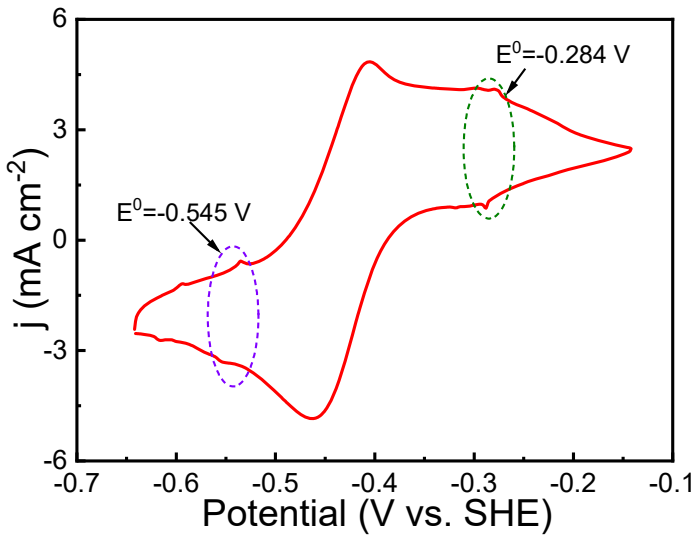


Fig. S6 CVs of MVCl_2 (10 mM) in 1 M NaCl solution containing 50 mM CuCl_2 on the bare GC electrode at 50 mV s^{-1} .

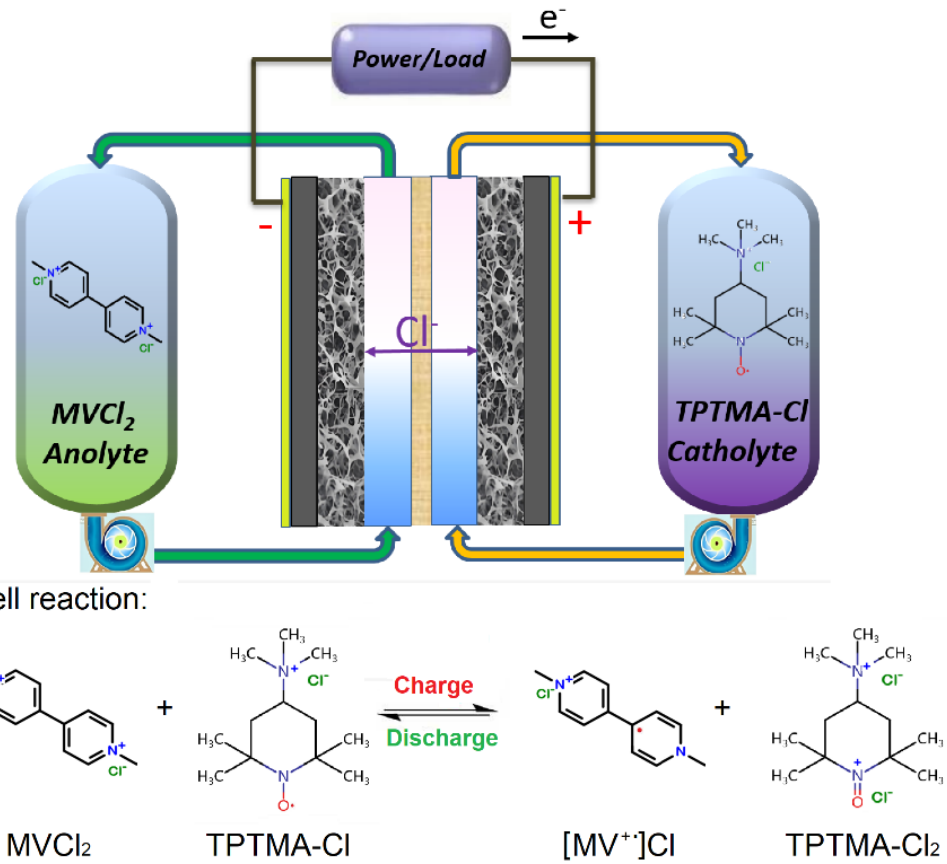


Fig. S7 A schematic representation of the pH-neutral $\text{MVCl}_2/\text{TPTMA-Cl}$ AORFB and its overall cell reaction.

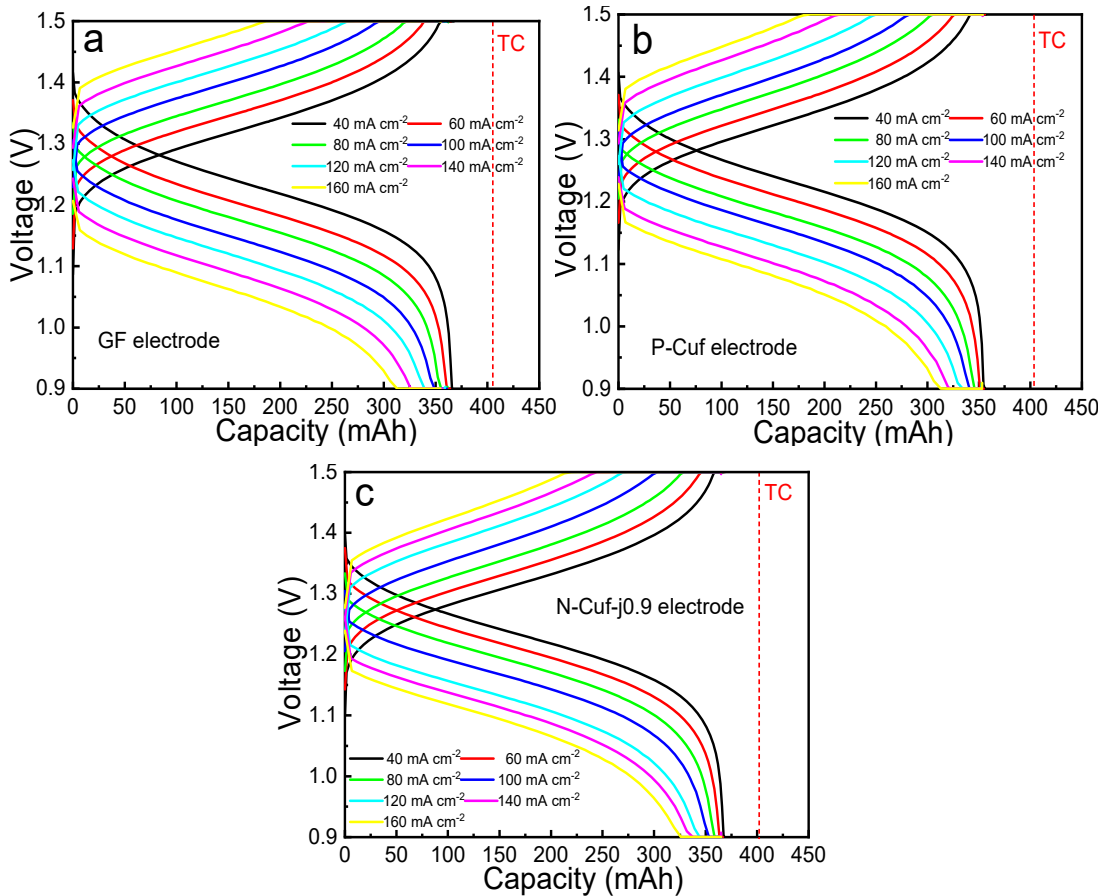


Fig. S8 Charge-discharge curves of the 1 M MVCl₂//TPTMA-Cl AORFB cell with the GF (a), P-Cuf (b), and N-Cuf-j0.9 (c) anodes, respectively, collected at various current densities.

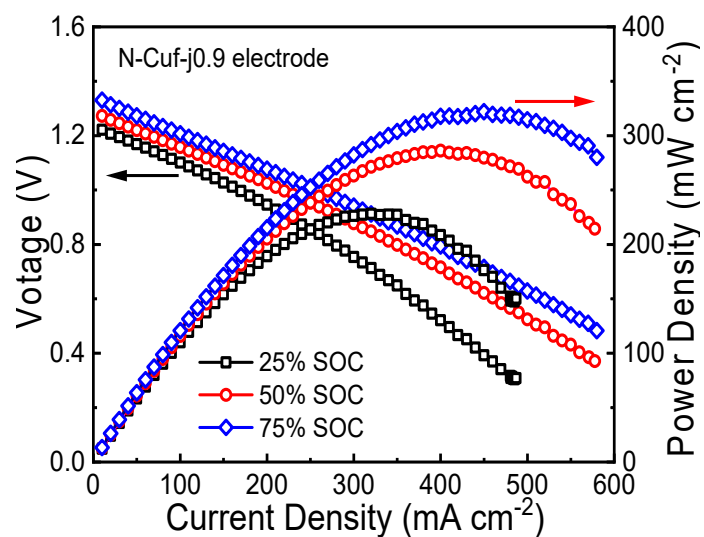


Fig. S9 Polarization and power density data of the 1 M MVCl₂//TPTMA-Cl cell with N-Cuf-j0.9 anode collected at 25%, 50% and 75% SOC.

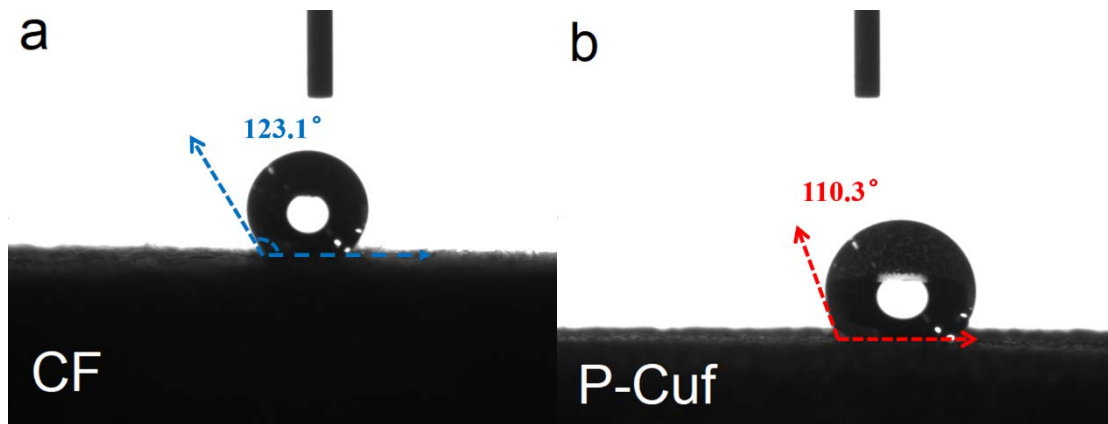


Fig. S10 The contact angle of water on the GF (a) and P-Cuf (b) surface.

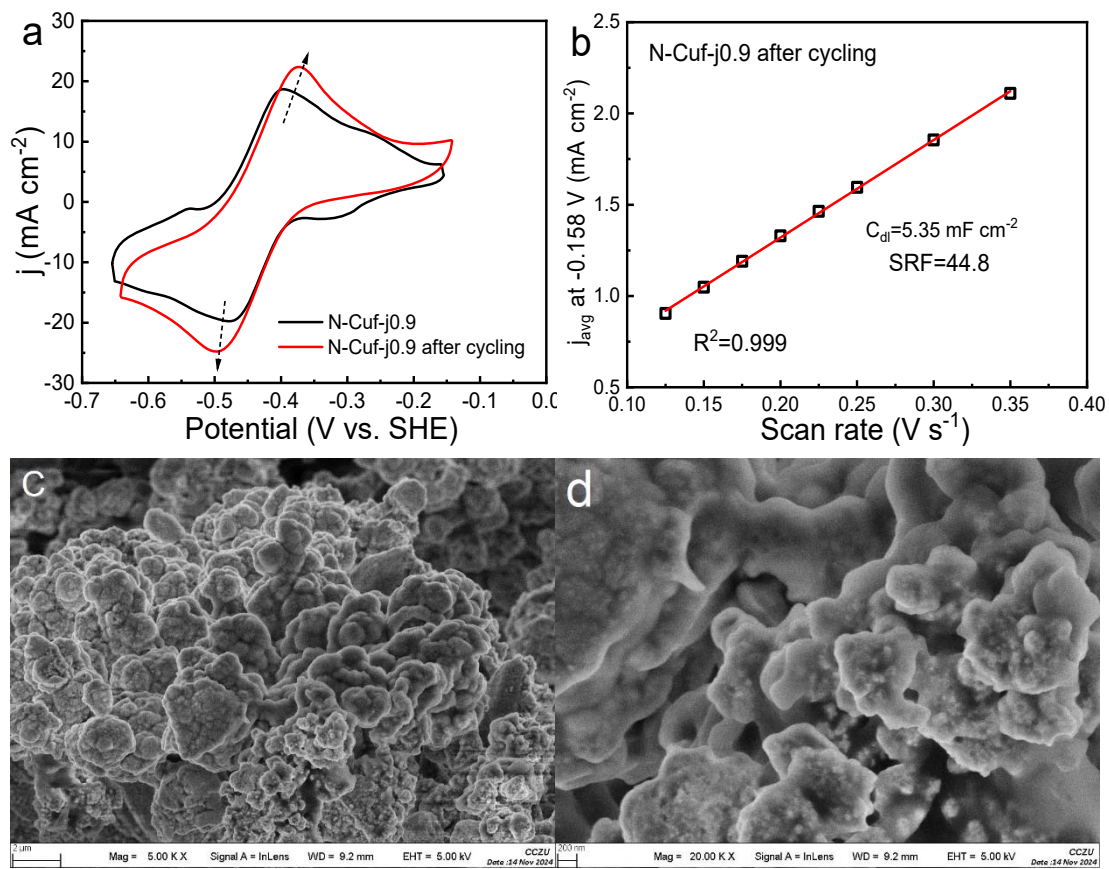


Fig. S11 Post analyses for the N-Cuf-j0.9 electrode. (a) CVs of MVCI_2 (10 mM) in 1 M NaCl electrolyte at 50 mV s⁻¹ on the N-Cuf-j0.9 electrode before and after 500 cycles. (b) Average magnitude of oxidative and reductive currents at -0.158 V vs. SHE for the N-Cuf-j0.9 electrode in 0.5 M KHCO_3 electrolyte as a function of scan rate ranging

from 125-350 mV s⁻¹. The red line is a linear fit to the points used to extract the non-Faradaic capacitance. (c-d) SEM images of the N-Cuf-j0.9 electrode after 500 cycles.

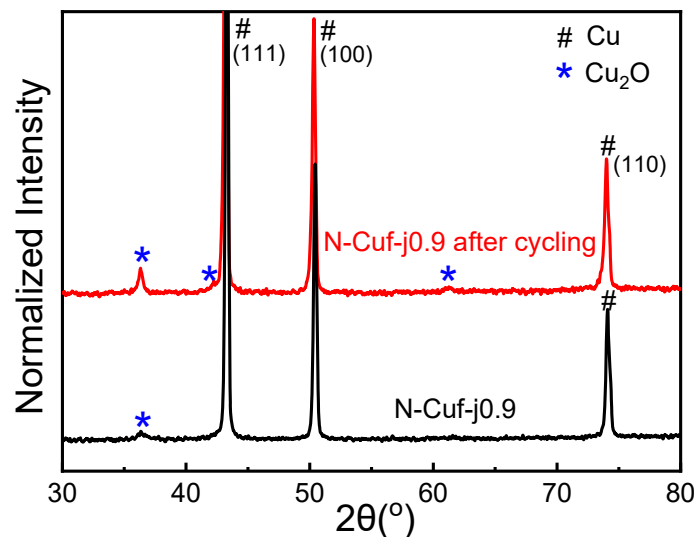


Fig. S12 XRD patterns of the N-Cuf-j0.9 before after cycling.

Table S2 The relative texture coefficients (RTCs) calculated by the Muresan method and peak current densities of oxidation and reduction reaction of MVCl₂ electrolyte ($j_{p,ox}$ and $j_{p,red}$) on the N-Cuf-j0.9 electrode before and after cycling.

Sample	N-Cuf-j0.9	N-Cuf-j0.9 after cycling
RTC(111)	57.56%	56.74%
RTC(100)	26.27%	26.61%
RTC(110)	16.16%	16.64%
$j_{p,ox}$ (mA cm ⁻²)	18.88	22.45
$j_{p,red}$ (mA cm ⁻²)	19.89	24.76

Table S3 The battery performance and cycling stability of viologen-based anolyte materials in AORFBs. P_{\max} , maximum power density. CFR, capacity fade rate. j, current density. C, concentration. SE, supporting electrolyte. NA, not applicable.

Viologen-based anolytes/ Catholytes	P_{\max} (mW cm ⁻²)	CFR (% per day)	Experimental conditions			
			Voltage (V)/j (mA cm ⁻²)	Anode/ Cathode	SE/Memb rane	C (M)/ Volume (mL)
MV/TPTMA This work	322(75% SOC)	0.103%	0.9-1.5/80	N-Cuf/GF	NH ₄ Cl/AE M	1/15
BTMAP-Vi/ TPP- TEMPO ^[R1]	135(100 %SOC)	0.161%	0.5-1.3/60	Carbon paper/Car bon paper	NH ₄ Cl/A MVN	0.5/5
BTMAP-Vi/ TMAP- TEMPO ^[R2]	134(100 %SOC)	0.648%	0.5- 1.5/100	Carbon paper/Car bon paper	NaCl/AM V	0.5/10
BTMAP-Vi/ TMAAcNH- TEMPO ^[R3]	NA	0.336%	0.7-1.8/50	Graphite plates/Gra phite plates	KCl/AEM	0.5/7
[PyrPV]Cl ₄ /Py r-TEMPO ^[R4]	317(100 %SOC)	4.56%	1.0-1.9/40	GF/GF	NaCl/DS V	0.2/5
MV/HO- TEMPO ^[R5]	NA	3.64%	0.5-1.7/60	GF/GF	NaCl/Sele mion	0.5/12
MV//TEMPT MA ^[R6]	NA	~0.4%	0.6-1.6/80	GF/GF	NaCl/FAA -3-PE-30	2/12
MV//FcNCl ^[R7]	125(full charge)	~0.33%	0.1-1.5/60	GF/GF	NaCl/AM V	0.7/11-13
[(NPr) ₂ V]Cl ₄ // N ^{Me} -TEMPO ^[R8]	134(100 %SOC)	~0.36%	0.3-1.7/60	GF/GF	NaCl/AE M	0.5/12
Dex-DiOH-Vi/ MMA- TEMPO ^[R9]	NA	~0%	0.5- 1.35/30	GF/GF	Not used/ AMVN	2.5/5
BPP- Vi/K ₄ Fe(CN) ₆ ^[R10]	~150(100 %SOC)	0.016%	0.4-1.1/40	Carbon paper/Car bon pape	NH ₄ OH/F umasep E- 620(K)	1/6.2

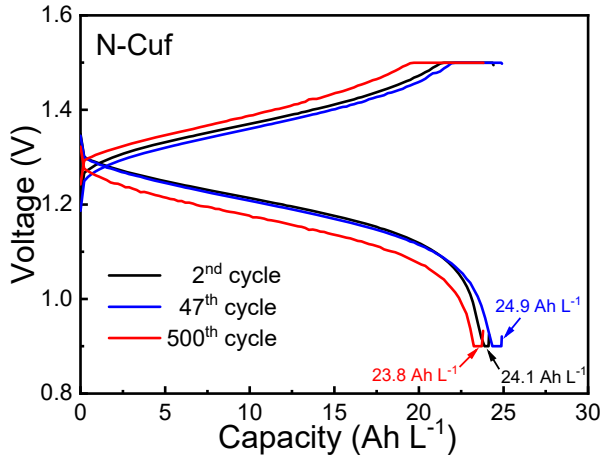


Fig. S13 Charge-discharge profiles of the N-Cuf cell under 80 mA cm^{-2} at the 2nd, 47th, and 500th cycles, respectively.

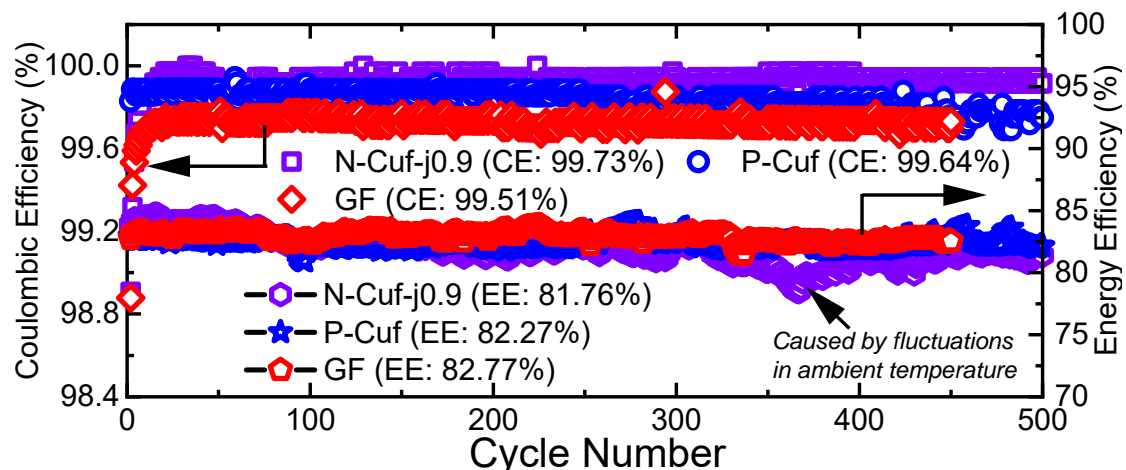


Fig. S14 The coulombic efficiency and energy efficiency profiles at 80 mA cm^{-2} for 1 M $\text{MVCl}_2/\text{TPTMA-Cl}$ AORFB cells with the GF, P-Cuf and N-Cuf-j0.9 anodes, respectively, during long-term cycling. The average CE of the N-Cuf-j0.9 cell is 99.73%, which is higher than those of the P-Cuf cell (99.64%) and the GF cell (99.51%). However, the average EE of the N-Cuf-j0.9 cell is found to be 81.76%, lower than those of the P-Cuf cell (82.27%) and the GF cell (82.77%), which is due to fluctuations in ambient temperature during long-term cycles.

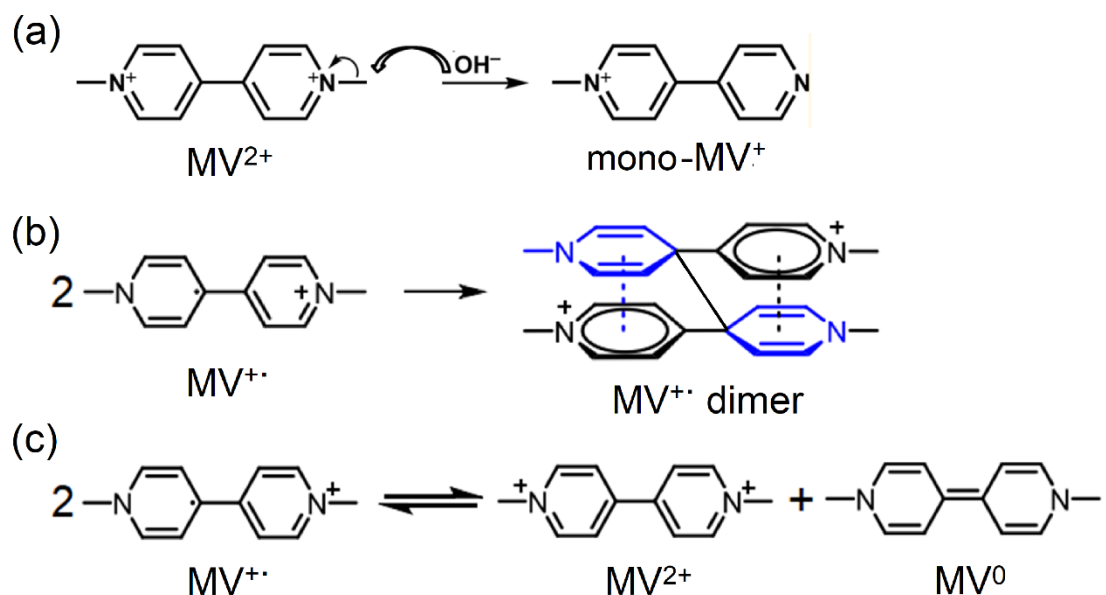


Fig. S15 Side reactions of MV and its reduced state ($\text{MV}^{+ \cdot}$). (a) dealkylation, (b) dimerization, and (c) disproportionation.

References

- [R1] G. Tang, W. Wu, Y. Liu, K. Peng, P. Zuo, Z. Yang, T. Xu, Nat. Commun., 2025, 16, 47.
- [R2] Y. Liu, M.-A. Goulet, L. Tong, Y. Liu, Y. Ji, L. Wu, R. G. Gordon, M. J. Aziz, Z. Yang, T. Xu, Chem 2019, 5, 1861-1870.
- [R3] H. Fan, W. Wu, M. Ravivarma, H. Li, B. Hu, J. Lei, Y. Feng, X. Sun, J. Song, T. L. Liu, Adv Funct Mater. 2022, 32, 2203032.
- [R4] M. Pan, L. Gao, J. Liang, P. Zhang, S. Lu, Y. Lu, J. Ma, Z. Jin, Adv. Energy Mater. 2022, 12, 2103478.
- [R5] T. Liu, X. Wei, Z. Nie, V. Sprenkle, W. Wang, Adv. Energy Mater. 2016, 6, 1501449.
- [R6] T. Janoschka, N. Martin, M. D. Hager, U. S. Schubert, Angew. Chem. Int. Ed.

2016, 55, 1-5.

[R7] B. Hu, C. DeBruler, Z. Rhodes, T. L. Liu, J. Am. Chem. Soc. 2017, 139, 1207-1214.

[R8] B. Hu, Y. Tang, J. Luo, G. Grove, Y. Guo, T. L. Liu, Chem. Commun. 2018, 54, 6871-6874.

[R9] P. T. Sullivan, H. Liu, X.-L. Lv, S. Jin, W. Li, D. Feng, Adv. Energy Mater. 2023, 13, 2203919.

[R10] S. Jin, E. M. Fell, L. Vina-Lopez, Y. Jing, P. W. Michalak, R. G. Gordon, M. J. Aziz, Adv. Energy Mater. 2020, 10, 2000100.